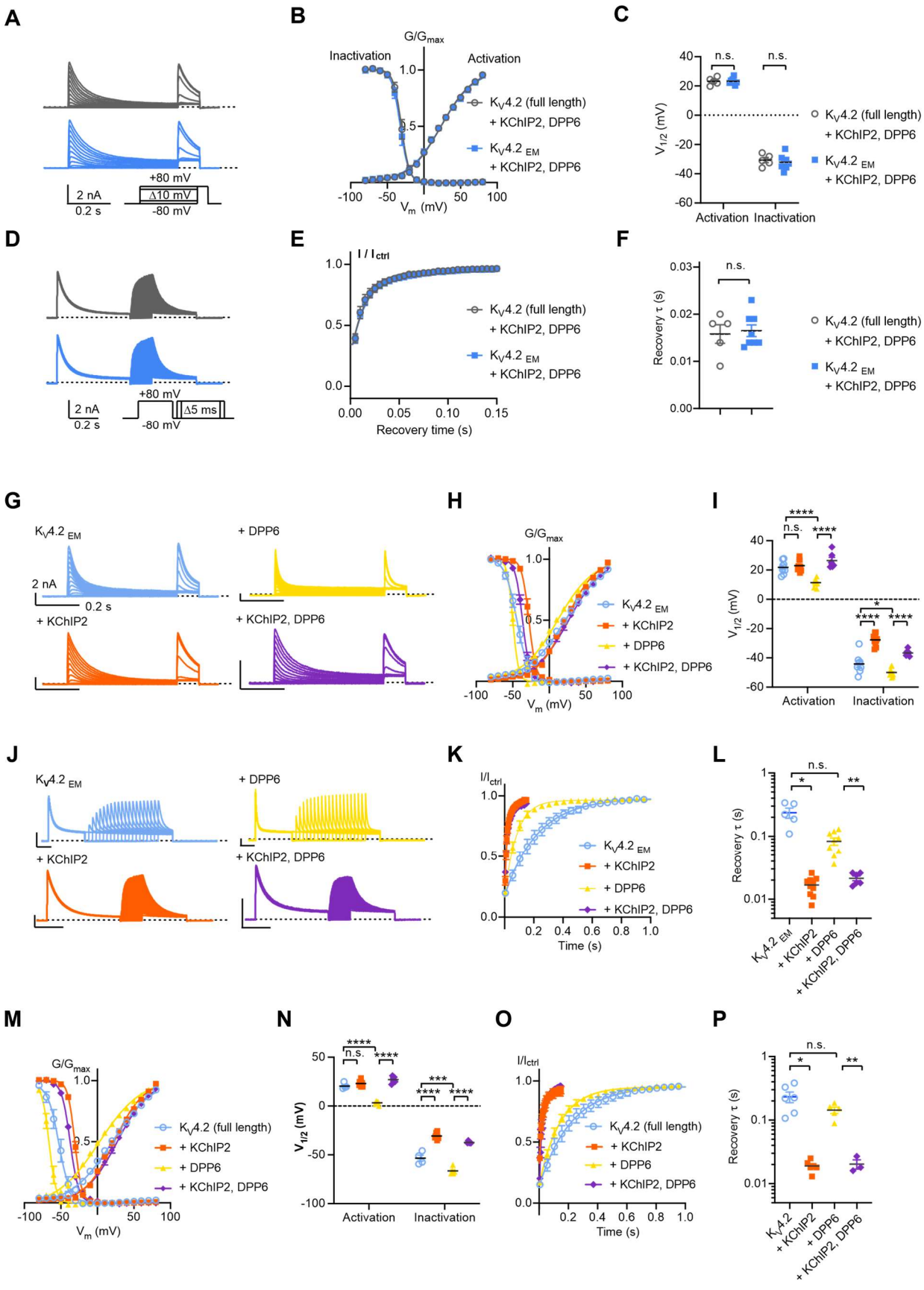
A
+80 mV
2 nA
0.2 s
Δ10 mV
-80 mV
B
G/Gmax
Inactivation
Activation
1.0
0.5
-100 -50 50 100
Vm (mV)
KV4.2 (full length)
+ KChIP2, DPP6
KV4.2 EM
+ KChIP2, DPP6
C
n.s.
n.s.
V1/2 (mV)
40
20
0
-20
-40
-60
Activation Inactivation
KV4.2 (full length)
+ KChIP2, DPP6
KV4.2 EM
+ KChIP2, DPP6
D
+80 mV
2 nA
0.2 s
Δ5 ms
-80 mV
E
I / Ictrl
1.0
0.5
0.0
0.00 0.05 0.10 0.15
Recovery time (s)
KV4.2 (full length)
+ KChIP2, DPP6
KV4.2 EM
+ KChIP2, DPP6
F
n.s.
Recovery τ (s)
0.03
0.02
0.01
0.00
KV4.2 (full length)
+ KChIP2, DPP6
KV4.2 EM
+ KChIP2, DPP6
G
KV4.2 EM
2 nA
0.2 s
+ DPP6
+ KChIP2
+ KChIP2, DPP6
H
G/Gmax
1.0
0.5
-100 -50 50 100
Vm (mV)
KV4.2 EM
+ KChIP2
+ DPP6
+ KChIP2, DPP6
I
****
n.s.
****
40
20
0
-20
-40
-60
V1/2 (mV)
*
****
****
Activation
Inactivation
J
KV4.2 EM
+ DPP6
+ KChIP2
+ KChIP2, DPP6
K
I/Ictrl
1.0
0.5
0.0
0.2 0.4 0.6 0.8 1.0
Time (s)
KV4.2 EM
+ KChIP2
+ DPP6
+ KChIP2, DPP6
L
n.s.
*
**
1
0.1
0.01
Recovery τ (s)
KV4.2 EM
+ KChIP2
+ DPP6
+ KChIP2, DPP6
M
G/Gmax
1.0
0.5
-100 -50 50 100
Vm (mV)
KV4.2 (full length)
+ KChIP2
+ DPP6
+ KChIP2, DPP6
N
****
n.s.
****
50
0
-50
-100
V1/2 (mV)
***
****
****
Activation
Inactivation
O
I/Ictrl
1.0
0.5
0.0
0.2 0.4 0.6 0.8 1.0
Time (s)
KV4.2 (full length)
+ KChIP2
+ DPP6
+ KChIP2, DPP6
P
n.s.
*
**
1
0.1
0.01
Recovery τ (s)
KV4.2
+ KChIP2
+ DPP6
+ KChIP2, DPP6

Figure S1. Electrophysiological analyses of $K_V4.2_{EM}$ and $K_V4.2$ (full length) activation, inactivation and modulation by KChIP2 and DPP6, Related to Figure 1

(A) Representative whole-cell recording traces of $K_V4.2$ (full length)/KChIP2/DPP6 (gray trace) and $K_V4.2_{EM}$/KChIP2/DPP6 (blue trace).

(B) Steady-state activation and inactivation curves from recordings as in (A). Data shown are mean ± SEM.

(C) Scatter plot showing half-activation and half-inactivation voltages ($V_{1/2}$) from recordings as in (B). Individual data points and mean values (black lines) are shown. n.s., not significant, as assessed by Welch's *t*-test.

(D) Representative whole-cell recording traces of $K_V4.2$ channel complexes, showing the channel recovery from inactivation.

(E) Time courses of channels recovering from inactivation from recordings as in (D). Data shown are mean ± SEM.

(F) Scatter plot showing recovery time constants (τ) from recordings as in (E). Mean values (black lines) and SEM (whiskers) are shown. n.s., not significant, as assessed by Welch's *t*-test.

(G) Representative recording traces of $K_V4.2_{EM}$ alone or with auxiliary subunits KChIP2 and DPP6.

(H) Steady-state activation and inactivation curves from recordings as in (G). Data shown are mean ± SEM.

(I) Scatter plot showing half-activation and half-inactivation voltages ($V_{1/2}$). Individual data points and mean values (horizontal black lines) are shown. *$p < 0.05$, ****$p < 0.0001$, n.s., not significant, as assessed by Tukey's tests following one-way ANOVA.

(J) Representative recording traces of $K_V4.2$ channel complexes, showing the channel recovery from inactivation.

(K) Time courses of channels recovering from inactivation from recordings as in (J). Data shown are mean ± SEM.

(L) Scatter plot showing recovery time constants (τ) from recordings as in (K). Individual data points and mean values (horizontal black lines) are shown. *$p < 0.05$, **$p < 0.01$, n.s., not significant, as assessed by Dunnett's tests following Brown-Forsythe ANOVA test.

(M) Steady-state activation and inactivation curves of $K_V4.2$ (full length) alone or with auxiliary subunits KChIP2 and DPP6. Data shown are mean ± SEM.

(N) Scatter plot showing half-activation and half-inactivation voltages ($V_{1/2}$). Individual data points and mean values (horizontal black lines) are shown. ***$p < 0.001$, ****$p < 0.0001$, n.s., not significant, as assessed by Tukey's tests following one-way ANOVA.

(O) Time courses of $K_V4.2$ (full length) alone, or with auxiliary subunits KChIP2 and DPP6, recovering from inactivation. Data shown are mean ± SEM.

(P) Scatter plot showing recovery time constants (τ) from recordings as in (I). Individual data points and mean values (horizontal black lines) are shown. *$p < 0.05$, **$p < 0.01$, n.s., not significant, as assessed by Dunnett's tests following Brown-Forsythe ANOVA test.

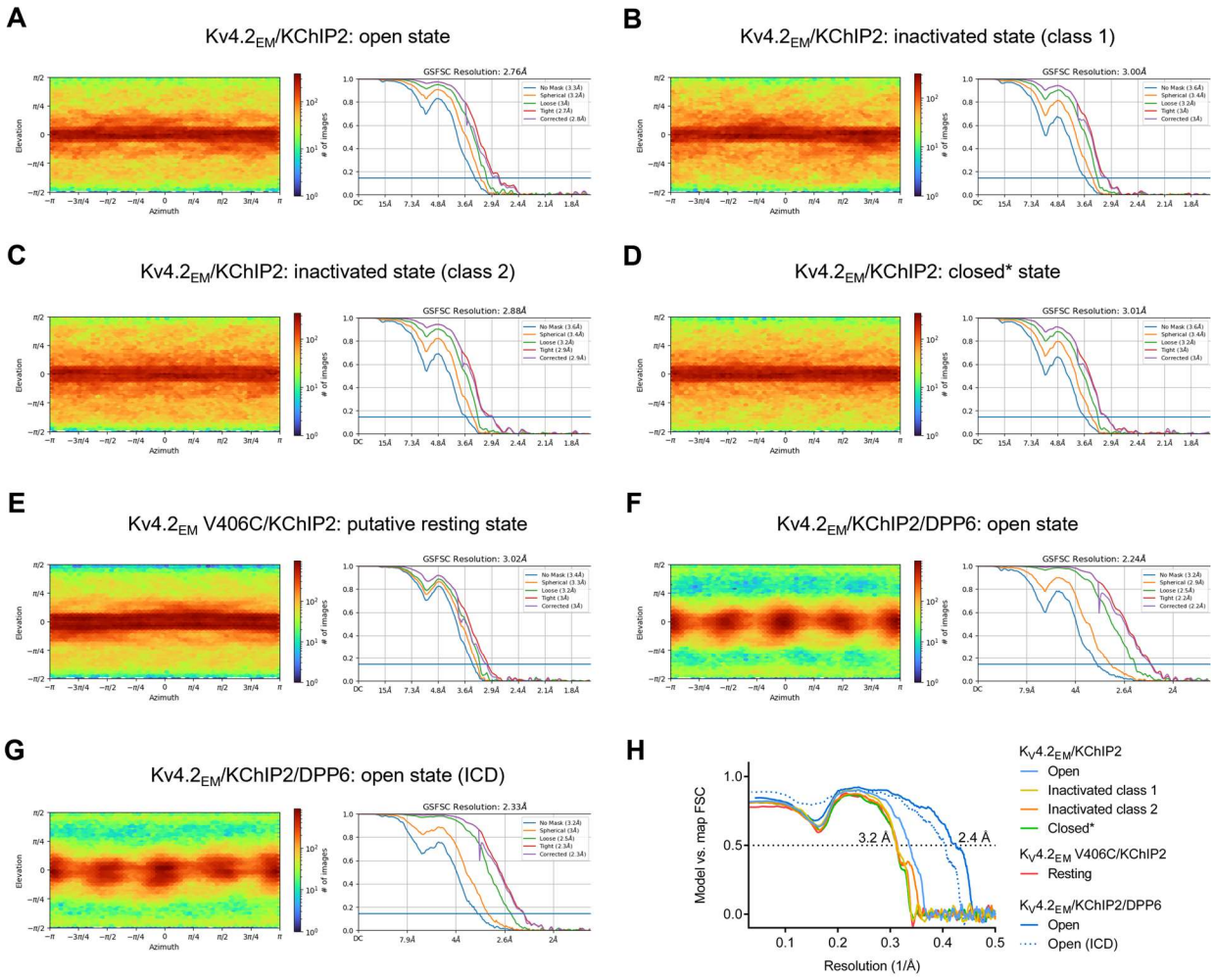

Figure S2. Cryo-EM analyses of K_V4 channel complexes in different states, Related to Figures 1, 2, 3, 6, and 7

(A) to (G) Left, angular distribution of particles for the final 3D reconstruction. Right, Fourier shell correlation (FSC) curves between two half maps. In (A) to (F), the reconstructions are focused on the transmembrane domains. In (G), the reconstruction is focused on the intracellular domains (ICD).

(H) Fourier shell correlation (FSC) curves between maps and final 3D reconstructions.

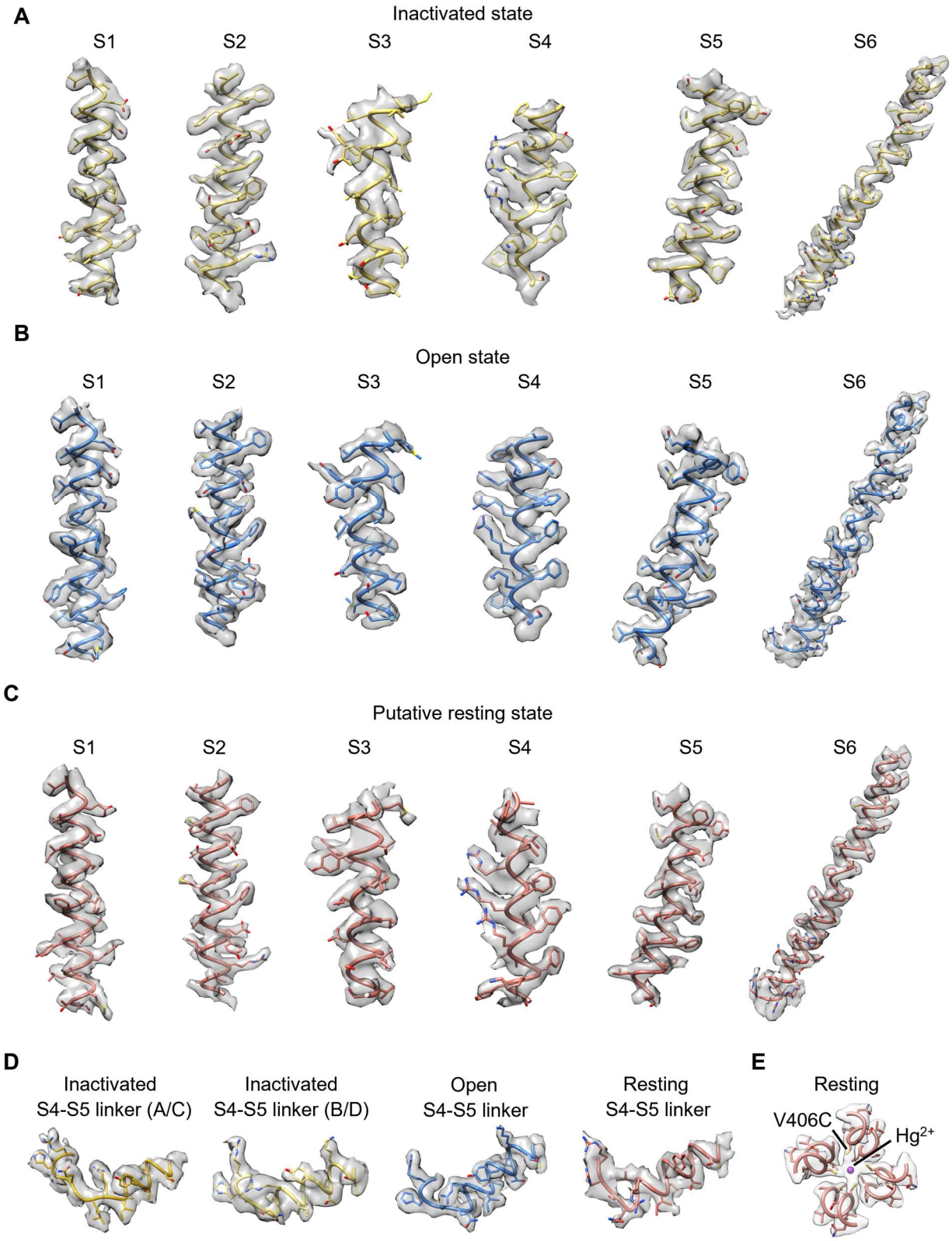
A
Inactivated state
S1
S2
S3
S4
S5
S6
B
Open state
S1
S2
S3
S4
S5
S6
C
Putative resting state
S1
S2
S3
S4
S5
S6
D
Inactivated
S4-S5 linker (A/C)
Inactivated
S4-S5 linker (B/D)
Open
S4-S5 linker
Resting
S4-S5 linker
E
Resting
V406C
Hg2+

Figure S3. Representative cryo-EM density of K_V4 segments in different states, Related to Figures 1, 2, 3, 6, and 7

(A) S1 to S6 helices in the inactivated state.

(B) S1 to S6 helices in the open state.

(C) S1 to S6 helices in the putative resting state.

(D) S4-S5 linkers in different states.

(E) Hg^{2+} crosslinking on K_V4 V406C in the putative resting state

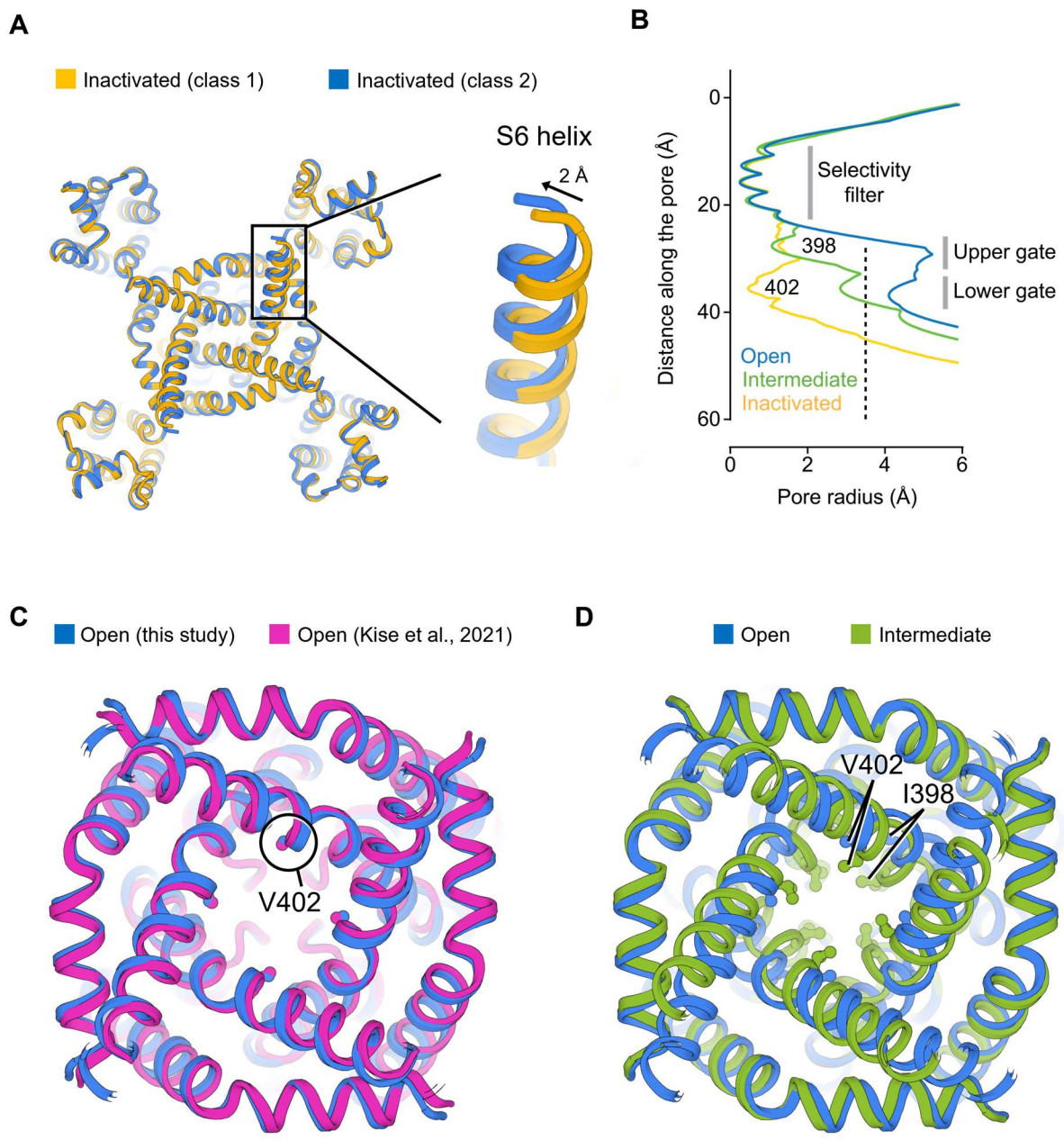

Figure S4. Structural comparisons of K_V4 in different states, Related to Figures 2 and 3

(A) Comparison of the inactivated class 1 and class 2.

(B) Radius of the pore in different states. The radius is plotted as a function of the distance along the pore axis. The minimal pore radius for hydrated K^+ ions to pass through (3.5 Å) is highlighted by a dash line.

(C) Comparison of the open pore structures from this study and from a previous report (Kise et al., 2021) (PDB: 7E7Z)

(D) Comparison of the pore structures in the open and intermediate states. Note that in the intermediate state, both I398 and V402 flip toward the conducting pathway and block the pore.

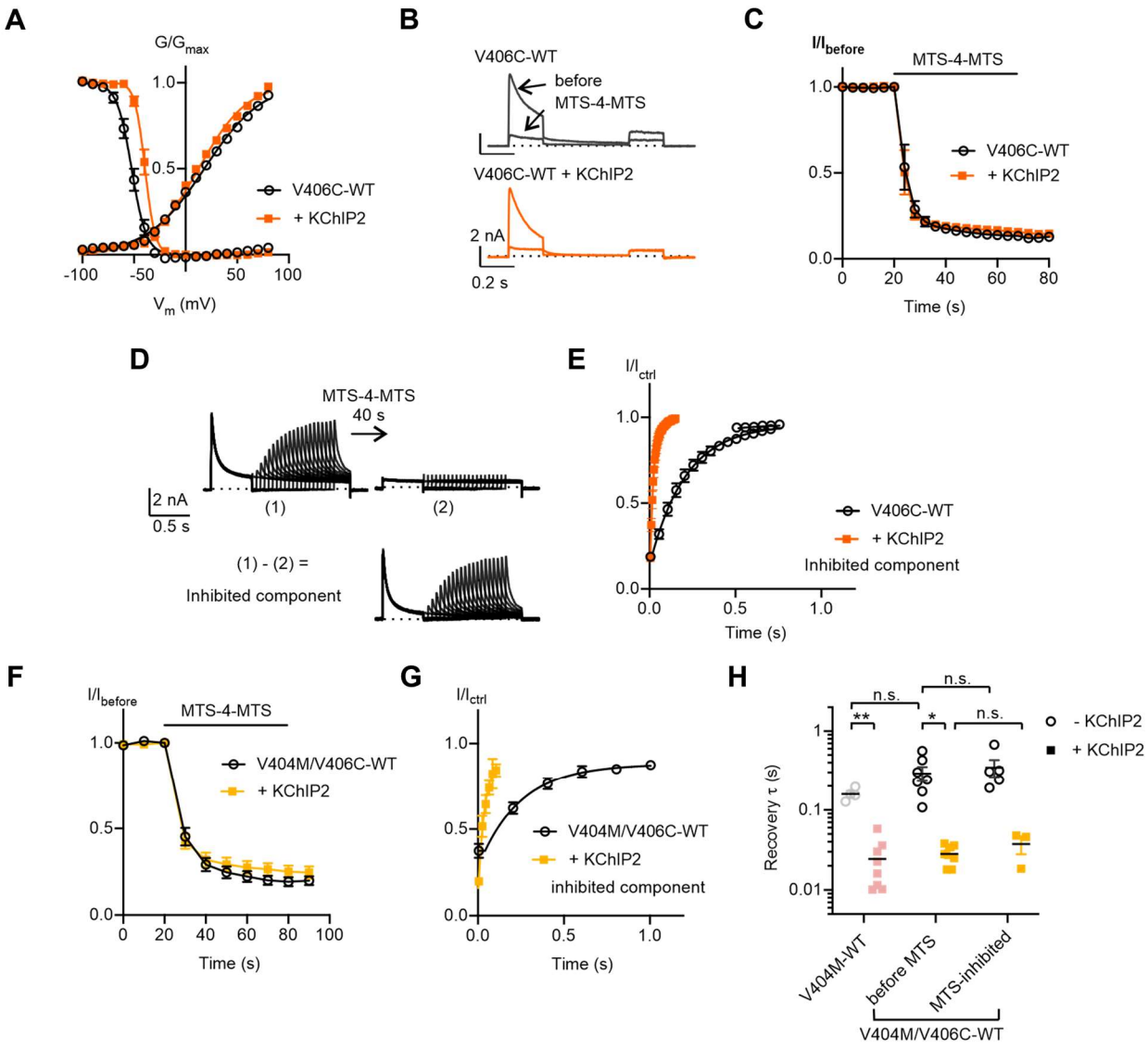

Figure S5. Electrophysiological analyses of K_V4.2 tandem constructs, Related to Figure 4

(A) Steady-state activation and inactivation curves of the V406C-WT channels. Data shown are mean ± SEM.

(B) Representative traces of V406C-WT channels upon MTS-4-MTS treatment, in the absence or presence of KChIP2.

(C) Time courses of V406C-WT current responses to MTS-4-MTS treatment. The current magnitudes were normalized to that at the sweep before treatment (I/I_{before}) for each cell. Data shown are mean ± SEM.

(D) Representative whole-cell recording traces of V406C-WT channels, showing the channel recovery from inactivation. The difference in currents before and after treatment is defined as the MTS-4-MTS inhibited component.

(E) Time courses of V406C-WT channels recovering from inactivation from recordings as in (D). The inhibited component is used for analysis. Data shown are mean ± SEM.

(F) Time courses of V404M/V406C-WT current responses to MTS-4-MTS treatment. The current magnitudes were normalized to that at the sweep before treatment (I/I_{before}) for each cell. Data shown are mean ± SEM.

(G) Time courses of V404M/V406C-WT channels recovering from inactivation. The inhibited component is used for analysis. Data shown are mean ± SEM.

(H) Scatter plot showing recovery time constants (τ) of V404M/V406C-WT channels. Individual data points and mean values (horizontal black lines) are shown. *$p < 0.05$, **$p < 0.01$, n.s., not significant, as assessed by Dunnett's tests following Brown-Forsythe ANOVA test.

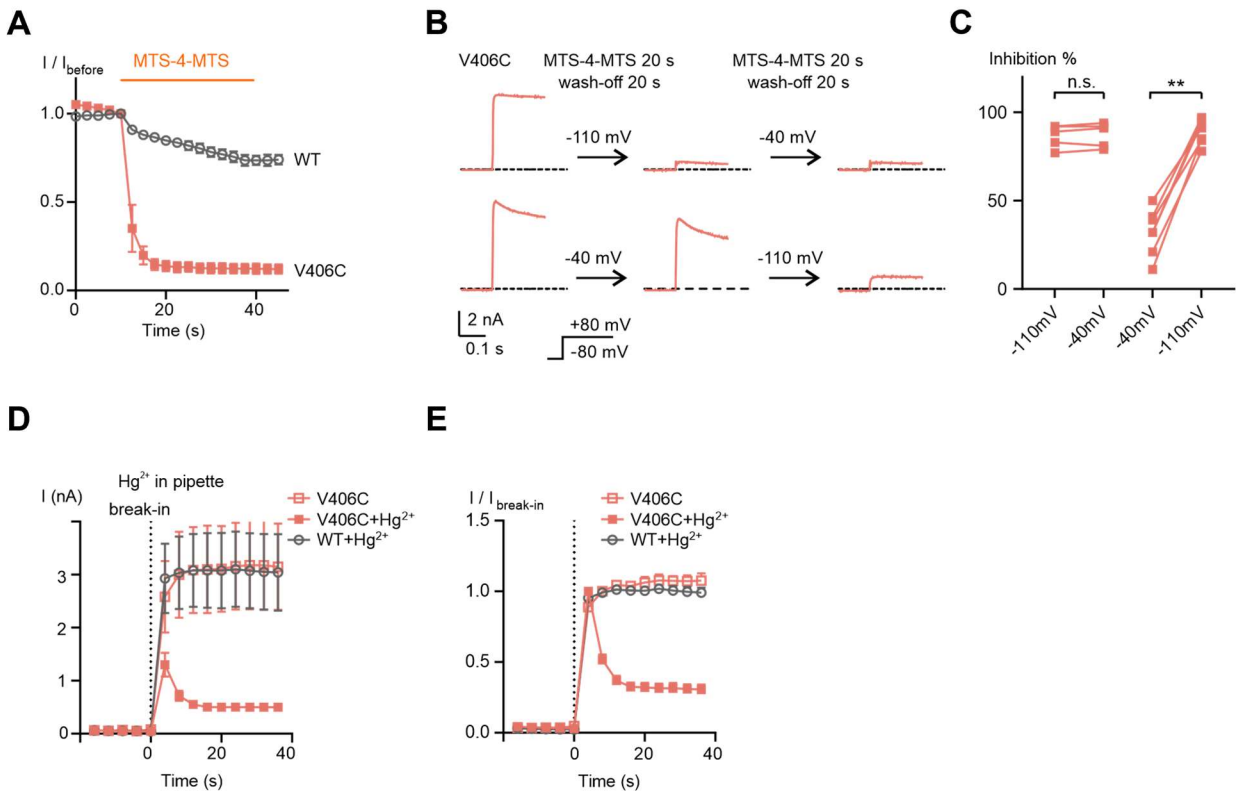

Figure S6. Crosslinking of K_V4 V406C by MTS-4-MTS or Hg^{2+}, Related to Figure 5

(A) Time courses of current responses to MTS-4-MTS treatment. The current magnitudes were normalized to that at the sweep before treatment (I/I_{before}) for each cell. Data shown are mean ± SEM.

(B) Representative traces of K_V4 V406C upon MTS-4-MTS treatment, showing the state-dependence of MTS-4-MTS inhibition. Currents were evoked by a depolarizing step to +80 mV from -80 mV. After recording for 2 to 3 sweeps, the membrane potential was held at the indicated potentials for 60 seconds, during which MTS-4-MTS was perfused for 20 s and then normal extracellular solution was perfused for another 20 s, followed by subsequent recordings with the same protocol.

(C) Summary of MTS-4-MTS inhibition. Two sequential recordings from the same cell are connected by a line. *$p < 0.05$, n.s., not significant, as assessed by Dunnett's test following Kruskal-Wallis test.

(D) and (E) Time courses of changes in K_V4 peak currents in the absence or presence Hg^{2+}. The recordings start before breaking in (before the 0 s time point). In (E), currents were normalized to that at the first sweep after breaking in ($I/I_{break\text{-}in}$). Data shown are mean ± SEM.

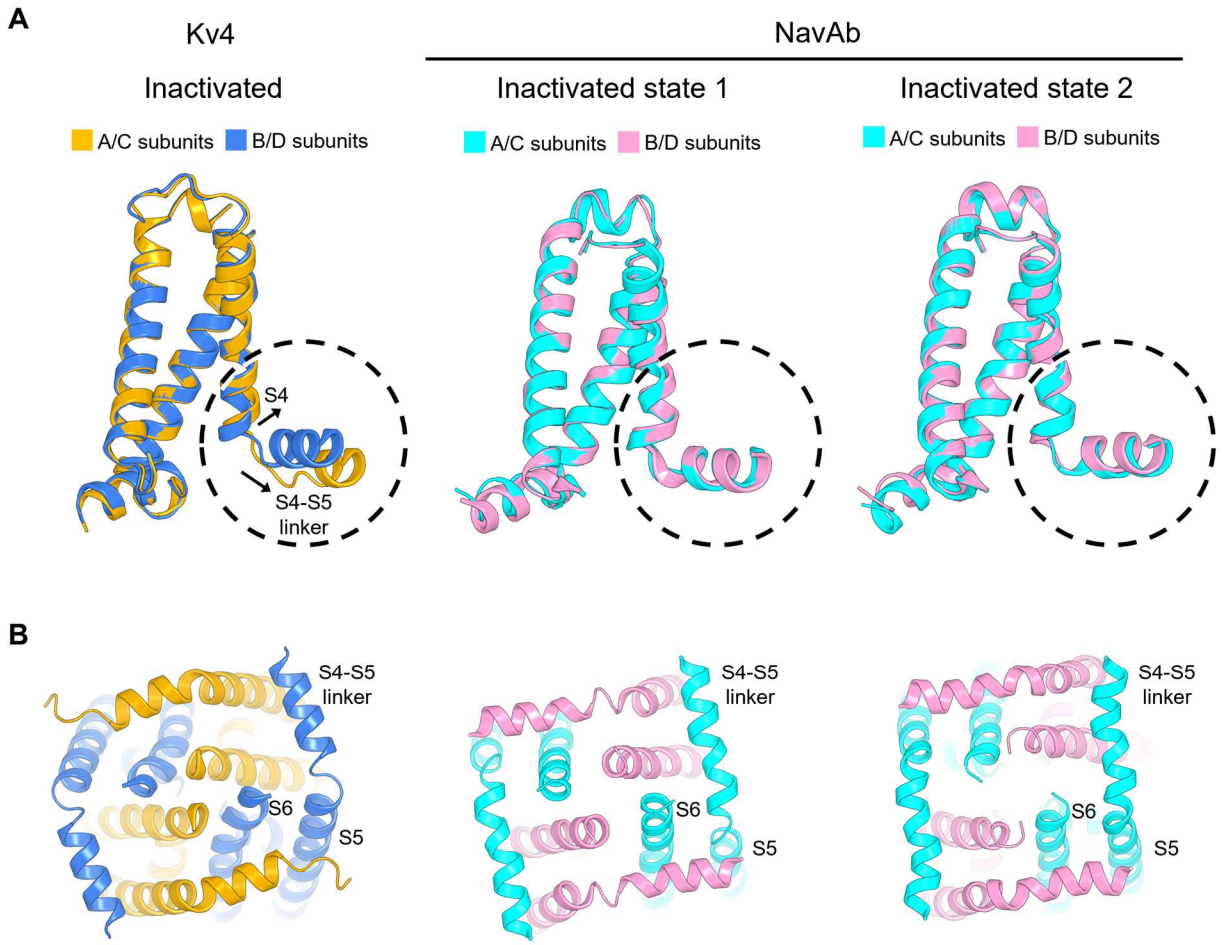

Figure S7. Structural comparisons of K_V4 and Na_VAb in inactivated states, Related to Figures 1, 2, and 3

(A) Voltage sensing domains of Kv4 and NavAb in inactivated states.

(B) Pore domains of Kv4 and NavAb in inactivated states, viewed from the intracellular side.

	$K_V4.2_{EM}$ / KChIP2 Open	$K_V4.2_{EM}$ / KChIP2 Inactivated Class 1	$K_V4.2_{EM}$ / KChIP2 Inactivated Class 2	$K_V4.2_{EM}$ / KChIP2 Intermediate	$K_V4.2_{EM}$ V406C / KChIP2 Resting	$K_V4.2_{EM}$ / KChIP2 / DPP6 Open	$K_V4.2_{EM}$ / KChIP2 / DPP6 Intracellular region
Data collection and processing							
Magnification	105,000	105,000	105,000	105,000	105,000	105,000	105,000
Voltage (kV)	300	300	300	300	300	300	300
Electron exposure ($e^-/Å^2$)	76.4	76.4	76.4	76.4	69.6	85.9	85.9
Defocus range (μm)	0.6–1.6	0.6–1.6	0.6–1.6	0.6–1.6	0.6–1.6	0.6–1.6	0.6–1.6
Pixel size (Å)	0.826	0.826	0.826	0.826	0.826	0.826	0.826
Symmetry imposed	C4	C2	C2	C2	C4	C4	C4
Final particle images (no.)	214021	187073	210659	199309	486681	278343	278343
Map resolution (Å)	2.76	3.00	2.88	3.01	3.02	2.24	2.33
FSC threshold	0.143	0.143	0.143	0.143	0.143	0.143	0.143
Refinement							
Map sharpening B factor ($Å^2$)							
Model composition							
Nonhydrogen atoms	8004	8000	8000	8000	8005	8656	12344
Protein residues	1036	1036	1036	1036	1036	1128	1536
Ligands	4	4	4	4	5	4	16
B factors ($Å^2$)							
Protein	50.78	56.68	75.29	79.96	65.47	50.12	39.31
Ligand	31.47	23.89	29.61	27.60	58.76	19.02	53.76
R.m.s. deviations							
Bond lengths (Å)	0.004	0.006	0.004	0.003	0.004	0.006	0.004
Bond angles (°)	0.637	0.656	0.609	0.611	0.597	0.629	0.649
Validation							
MolProbity score	1.65	1.64	1.49	1.48	1.56	1.33	1.78
Clashscore	8.62	8.37	9.18	9.05	9.17	6.08	7.75
Poor rotamers (%)	0	0	0	0	0	0	1.8
Ramachandran plot							
Favored (%)	96.89	96.89	98.05	98.83	97.67	98.20	97.07
Allowed (%)	3.11	3.11	1.95	1.17	2.33	1.80	2.93
Disallowed (%)	0	0	0	0	0	0	0

Table S1. Cryo-EM data collection, refinement and validation statistics, Related to Figure 1